JOURNAL OF CATALYSIS **179,** 431–442 (1998)
ARTICLE NO. CA982178

Structure and Reactivity of PdO_x/ZrO_2 Catalysts for Methane Oxidation at Low Temperatures

Ken-ichiro Fujimoto, Fabio H. Ribeiro,[1] Miguel Avalos-Borja,* and Enrique Iglesia[2]

*Department of Chemical Engineering, University of California at Berkeley, and Materials Sciences Division, E. O. Lawrence Berkeley National Laboratory, Berkeley, California 94720–1462; *Institute of Physics, Universidad Nacional Autonoma, Ensenada, Baja California, Mexico*

Received February 4, 1998; revised June 1, 1998; accepted June 1, 1998

The kinetics of methane combustion at low temperatures are consistent with a Mars–van Krevelen redox mechanism involving the activation of methane on site pairs consisting of oxygen atoms and oxygen vacancies on the surface of PdO_x crystallites. H_2O strongly inhibits methane oxidation rates by titrating surface vacancies in a quasi-equilibrated adsorption–desorption step. Initial activation periods during methane oxidation are related to the presence of oxygen-deficient PdO_x crystallites, which contain stronger Pd–O oxygen bonds and increase their oxygen content during steady-state combustion reactions. Strong Pd–O bonds in small crystallites and in oxygen-deficient PdO_x also lead to the observed decrease in methane oxidation turnover rates as crystallite size decreases or as samples are treated at temperatures above those required for PdO-to-Pd decomposition.

Key Words: **methane combustion; Pd oxide catalysts.**

1. INTRODUCTION

Effluent streams from natural gas combustion processes contain small amounts of unconverted methane and residual carbon monoxide. Removal by postcombustion catalytic devices will require catalytic oxidation of methane at typical exhaust temperatures (600–700 K) in the presence of high CO_2 and H_2O concentrations. Low-temperature hydrocarbon combustion catalysts are also used in closed-coupled catalytic converters designed to minimize cold-start emissions in gasoline engines and in first-stage catalytic combustors for power generation (1,2).

Pd-based catalysts are very active in the complete oxidation of methane (3–9), but current catalysts based on supported PdO clusters require temperatures above 600 K and high Pd concentrations to convert methane in the presence of combustion products, which strongly inhibit catalytic methane oxidation reactions at low temperatures (9–11).

This study addresses the effects of Pd dispersion and oxidation–reduction treatments on the rate of methane combustion on PdO_x clusters supported on ZrO_2. We show that activating induction periods during catalytic oxidation of methane are related to equilibration of oxygen-deficient PdO species. A sequence of elementary reaction steps consistent with measured rate expressions and observed inhibition effects suggests that methane activation steps require vacancies in PdO_x, the density of which decreases with increasing Pd–O bond energy and H_2O concentration.

2. METHODS

Catalysts were prepared by incipient wetness impregnation of ZrO_2 (RC-100P, Daiichi Kigenso Kagaku Co., 16.5 $m^2\,g^{-1}$, air treatment at 1123 K, 10 h) with $Pd(NH_3)_2(NO_2)_2/HNO_3$ solutions (Tanaka Kikinzoku Kogyo Co.). Impregnated supports were dried in air at 373 K for 24 h. Some samples were treated in stagnant air by raising temperatures from ambient (RT) to 773 K at 5–10 K min^{-1} and holding for 24 h. Other samples were treated in flowing dry air (200–500 $cm^3\,min^{-1}$) by raising the temperature slowly to 773 K (0.5 K min^{-1} to 523 K, 10 K min^{-1} to 773 K) and holding for 24 h. These two methods led to different initial methane oxidation rates, but did not influence steady-state turnover rates on PdO_x/ZrO_2 catalysts, as discussed below.

The number of exposed Pd atoms was measured using H_2–O_2 titrations (12) after samples were reduced in H_2 (2-4 cm^3 H_2/g-s) at 373 K for 1 h and evacuated at 373 K for 1 h to remove chemisorbed hydrogen. O_2 chemisorption uptakes and titration of chemisorbed oxygen by H_2 were measured at 373 K and 2.7–11 kPa H_2 or O_2. Monolayer values were obtained by extrapolating isotherms to zero pressure. The number of exposed Pd metal atoms was calculated using reported stoichiometries [12]:

$$Pd + \tfrac{1}{2}O_2 \rightarrow PdO \qquad (O_2 \text{ chemisorption})$$

$$PdO + \tfrac{3}{2}H_2 \rightarrow PdH + H_2O \qquad (\text{titration of adsorbed oxygen by } H_2)$$

[1] Current address: Department of Chemical Engineering, Worcester Polytechnic Institute, Worcester, MA 01609.

[2] To whom correspondence should be addressed. E-mail: iglesia@cchem.berkeley.edu. Fax: 510–642–4778.

0021-9517/98 $25.00

Crystallite sizes were estimated from these dispersions by assuming hemispherical crystallites and a Pd surface density of 1.27×10^{19} m^{-2} (13,14).

X-ray diffraction (XRD) data were obtained using a Siemens D5000 diffractometer and Cu$K\alpha$ radiation. Broad diffraction lines for PdO (at $2\theta = 33.7°, 54.8°$) were detected in fresh catalysts with high Pd loadings (>3 wt%) after treatment in air at 773 K for 24 h. Corresponding PdO diffraction lines were not detected at lower Pd concentrations, suggesting that PdO clusters were noncrystalline or very small. Reduction in H_2 at 373 K and PdO decomposition above 1100 K led to Pd metal diffraction lines in fresh catalysts.

Temperature-programmed reduction (TPR) studies of PdO in H_2 were used to probe the stability of Pd–O bonds in reducing environments. These studies were carried out by increasing the temperature from 243 to 873 K at 3 K min^{-1} in a stream of 20% H_2/Ar (50 cm^3 min^{-1}). H_2 concentrations were obtained from thermal conductivity measurements of the effluent after the water formed during reduction was adsorbed onto a 13X molecular sieve held at room temperature.

Transmission electron microscopy samples were prepared by grinding catalysts with an agate mortar and pestle, mixing the fine powders with ethanol, and dispersing the mixtures ultrasonically for 0.1–0.2 h. A drop of this suspension was placed on a grid coated with a holey-carbon film and dried under a low-intensity lamp. Micrographs were obtained using a Jeol 2010 transmission electron microscope with a resolution of 0.2 nm. Standard bright- and dark-field imaging methods were used. Detailed electron microscopy studies were carried out only on samples with high Pd concentrations (4.1 wt%), because accurate statistics were not possible at lower Pd concentrations.

Methane oxidation rates were measured in a tubular reactor using a thin layer of catalyst (20–50 mg) held above acid-washed quartz wool. This configuration leads to hydrodynamics resembling a well-mixed reactor. Temperatures were measured with a K-type thermocouple placed within a quartz sheath touching the catalyst bed. Reactant mixtures (2% CH_4, 78% He, 20% O_2) were prepared by mixing He (Middleton Bay Airgas, 99.995%), 4% CH_4 in He (Alltair, primary standard grade, 99.97%), and O_2 (Air Liquide, 99.6%) using electronic mass flow controllers. Helium was purified using 13X molecular sieve and oxygen traps; all other gases were used without purification. Reactant and product concentrations were measured by gas chromatography (Hewlett–Packard 5890) using a Carbosphere packed column and a thermal conductivity detector.

Catalytic measurements were carried out by flowing He for 1 h at RT, increasing the temperature to 553 K at 8 K min^{-1}, holding for 0.2–0.3 h, and introducing CH_4/O_2 reactants. Effluent concentrations were measured after 0.1 h and then every 0.5 h. Interparticle heat and mass transfer restrictions were ruled out by diluting PdO_x/ZrO_2 with a tenfold excess of ZrO_2. Intraparticle transport restrictions were ruled out by varying catalyst pellet size. Reaction rates on diluted beds and on undiluted pellets 0.11–0.15 and <0.05 mm in diameter were similar (±5%). Reaction rates are reported at a constant methane conversion (5%); they are obtained by interpolating measured rates using kinetic rate expressions reported below and mole balance equations for well-stirred flow reactors. The inhibition by H_2O detected throughout the experimental conversion range (0.1–15%) requires that measured rates be corrected for varying water concentrations, even at very low conversions.

The rate of CO oxidation was measured at 393 K using a mixture of 1% CO in dry air purified by activated charcoal to remove metal carbonyls. After pretreatment or methane oxidation experiments, samples were cooled to RT and heated to 393 K at 4 K/min in a 20% O_2/He stream and held for 0.2–0.3 h before starting the flow of CO.

3. RESULTS AND DISCUSSION

3.1. Crystallite Size and Support Effects on Methane Combustion Turnover Rates

Steady-state methane oxidation turnover rates increased with increasing crystallite size on ZrO_2 and Al_2O_3 supports (Fig. 1), without significant changes in activation energy. Turnover rate values are compared at identical conversion levels (5%) to ensure that product concentrations (and their inhibition effects) are similar on all catalysts. Methane oxidation turnover rates at 553 K increase from 0.030 to 0.179 s^{-1} as the dispersion of PdO/ZrO_2 catalysts decreases from 0.381 to 0.120. These dispersion values correspond to approximate Pd metal crystallite diameters between 3 and 9 nm.

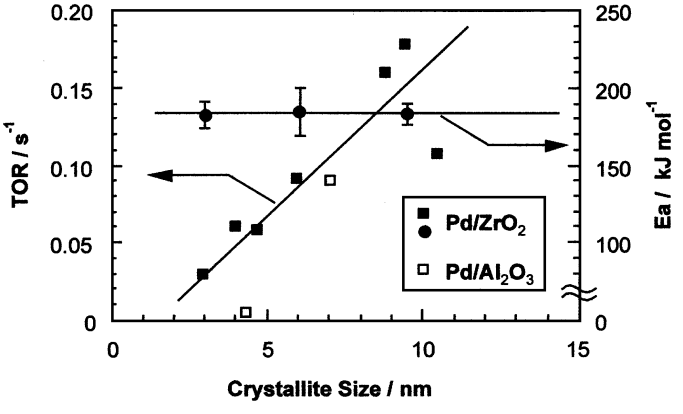

FIG. 1. Crystallite size effects on methane oxidation turnover rates (based on Pd dispersion measured by H_2–O_2 titration method) and activation energies (553 K, 2 kPa methane, 20 kPa O_2, 5% methane conversion; crystal size from H_2–O_2 titration dispersion values assuming quasi-spherical particles, 0.120–0.381 dispersion range).

These turnover rates ($3.0–17.9 \times 10^{-2}$ s^{-1}) are similar to those reported by Ribeiro *et al.* (9) and they are among the highest values reported under similar conditions. Incomplete activation during reaction may account for the lower turnover rates generally reported in other studies. Complete activation was confirmed in our study by showing that further activation does not occur when reactions are carried out at higher temperatures (673 K).

The underlying reasons for the wide range of turnover rate values reported on PdO catalysts (10^{-4}–10^{-1} s^{-1}) and for the observed effect of dispersion on turnover rates remain unclear. Dispersion values measured by chemisorptive titrations on catalysts reduced at low temperatures and used to calculate turnover rates may not reflect accurately the surface area of the PdO crystallites present during methane oxidation in excess oxygen. Turnover rate differences have also been attributed to PdO_x clusters with surface structures that vary sensitively with the identity of the support and the size of PdO_x clusters (7,8,15,16). Such structural modifications are detected by reactions that are structure sensitive. Incomplete catalyst activation, transport effects, and the widespread neglect of H_2O and CO_2 inhibition effects when comparing turnover rates at low but different conversions may have also contributed to the lack of agreement among reported turnover rates.

The strong influence of dispersion on methane oxidation turnover rates appears in a range of crystallite diameter for which surface structure should depend weakly on the size of PdO_x clusters (17). Also, the data in Fig. 1 show a linear relationship between turnover rate and crystallite diameter, even though size effects on structure should "saturate" as surface structures and turnover rates approach those on bulk oxides. The reasons for this apparent structure sensitivity remain unclear. Baldwin and Burch (6) reported turnover rates that vary by a factor of 100 among Pd/Al_2O_3 catalysts, but did not detect any correlation of these rates with PdO_x crystallite size. In contrast, Cullis and Willatt (4) did not observe strong effects of crystallite size on turnover rates. Hicks *et al.* (7,8) and Briot and Primet (15), however, reported higher turnover rates on larger Pd crystallites supported on alumina.

We consider two possibilities for the apparent structure sensitivity suggested by the data in Fig. 1 and by some of the previous studies (6–8,15). One proposal considers that small PdO_x crystallites (or those in closer contact with ZrO_2) contain stronger Pd–O bonds at their surface than larger ones. Stronger Pd–O bonds would decrease the stability and the surface density of oxygen vacancies, which are required for rate-determining C–H activation steps (Section 3.2). Indeed, the electronic properties and reducibility of oxide clusters on ZrO_2 change markedly within a wide crystallite size range (18) and domain size effects on electronic properties are ubiquitous in sulfide and oxide clusters (1–30 nm) used as quantum dot devices (19). Band gap energies in oxide semiconductors increase with decreasing domain size (20). Consequently, their reduction becomes more difficult as oxide particles become smaller, because the additional electron acquired during reduction must be placed into unoccupied states across a larger energy gap. The density and stability of oxygen vacancies involved in reduction–oxidation catalytic sequences will also decrease as band gap energies increase with decreasing PdO_x crystallite size. The binding energy of oxygen chemisorbed on supported Pd catalysts increases from 50 to 80 kcal/mol as the metal crystallite diameter decreases from 4 to 2 nm, suggesting strong size effects on Pd–O bond energies (21). Corresponding enthalpy data for Pd–O bond formation by reaction of O_2 with oxygen vacancies on oxygen-deficient PdO_x surfaces are not available as a function of crystallite size.

Another possibility is that PdO_x domains exist during methane oxidation as irregular oxide crystallites or grains with size or structure determined only by the mechanism of the oxidation process that forms PdO_x from Pd salts or Pd metal precursors, and not by the size or structure of such precursors. Then, PdO_x surface areas may be unrelated to the size of the Pd metal crystallites on which we base our turnover rate estimates. In this case, the use of hydrogen–oxygen titration methods, which require a mild reduction of PdO_x, could introduce an apparent crystallite size effect. Oxidation of Pd films during methane combustion can indeed lead to structural changes and to the formation of porous PdO films (22,23), but similar behavior has not been reported for supported Pd crystallites.

High-resolution transmission electron microscopy of 4.1 wt% PdO/ZrO_2 catalysts did not detect structural differences between PdO_x crystallites before (or after) methane oxidation and the corresponding metal crystallites, formed by mild reduction of PdO (at 373 K) and used in H_2–O_2 titration measurements. The average PdO crystallite in fresh samples (Fig. 2a) was 6 nm; this value increased slightly to about 7 nm after mild reduction treatments (Fig. 2b). The crystallite diameter calculated from titration measurments assuming hemispherical crystallites for this sample was 10.5 nm. Pd metal particles formed by mild reduction of PdO at 373 K appear to be slightly denser than corresponding PdO crystallites, but neither coalescence of PdO crystallites during reduction nor fragmentation of Pd metal during oxidation in air at 773 K is apparent from the micrographs in Figs. 2a and 2b. Pd and PdO crystallites are quasi-spherical and neither Pd nor PdO appears to wet the ZrO_2 surface.

We conclude that no significant agglomeration of PdO_x crystallites occurs during mild reduction at 373 K. H_2–O_2 titration methods on mildly reduced PdO samples provide dispersion values that are at least proportional to the dispersion of PdO before and after methane oxidation reactions. Thus, the observed effects of crystallite size are not caused by artifacts introduced by the mild reduction of PdO_x

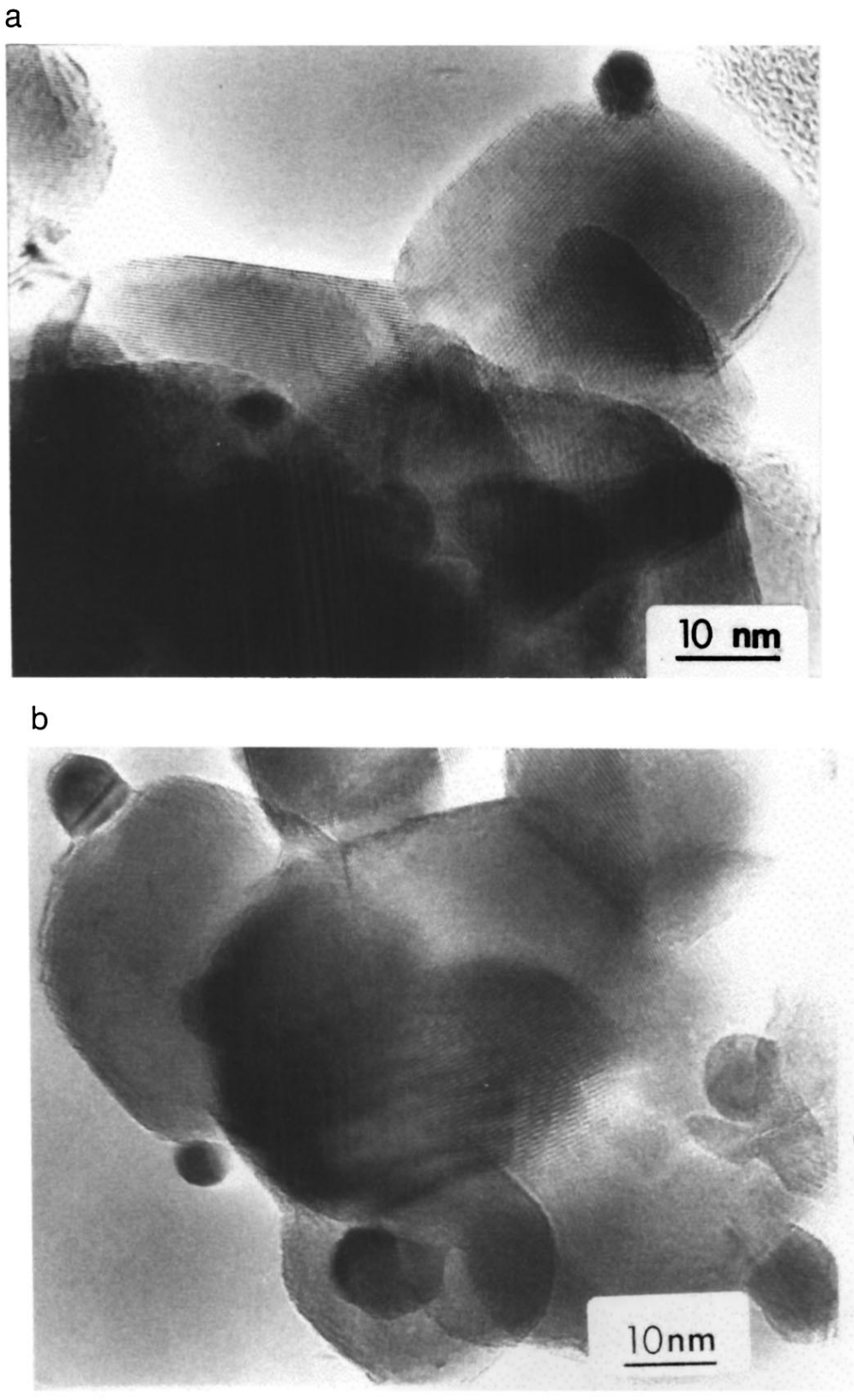

FIG. 2. Transmission electron micrographs of 4.1 wt% Pd/ZrO_2 samples after various pretreatment procedures: (a) fresh PdO/ZrO_2 catalyst; (b) fresh catalyst after reduction in H_2 at 373 K for 1 h; (c) PdO/ZrO_2 after methane combustion for 24 h at 553 K; (d) fresh catalyst treated in air at 1123 K and quenched in He to room temperature; (e) catalyst in (d) after air treatment at 973 K.

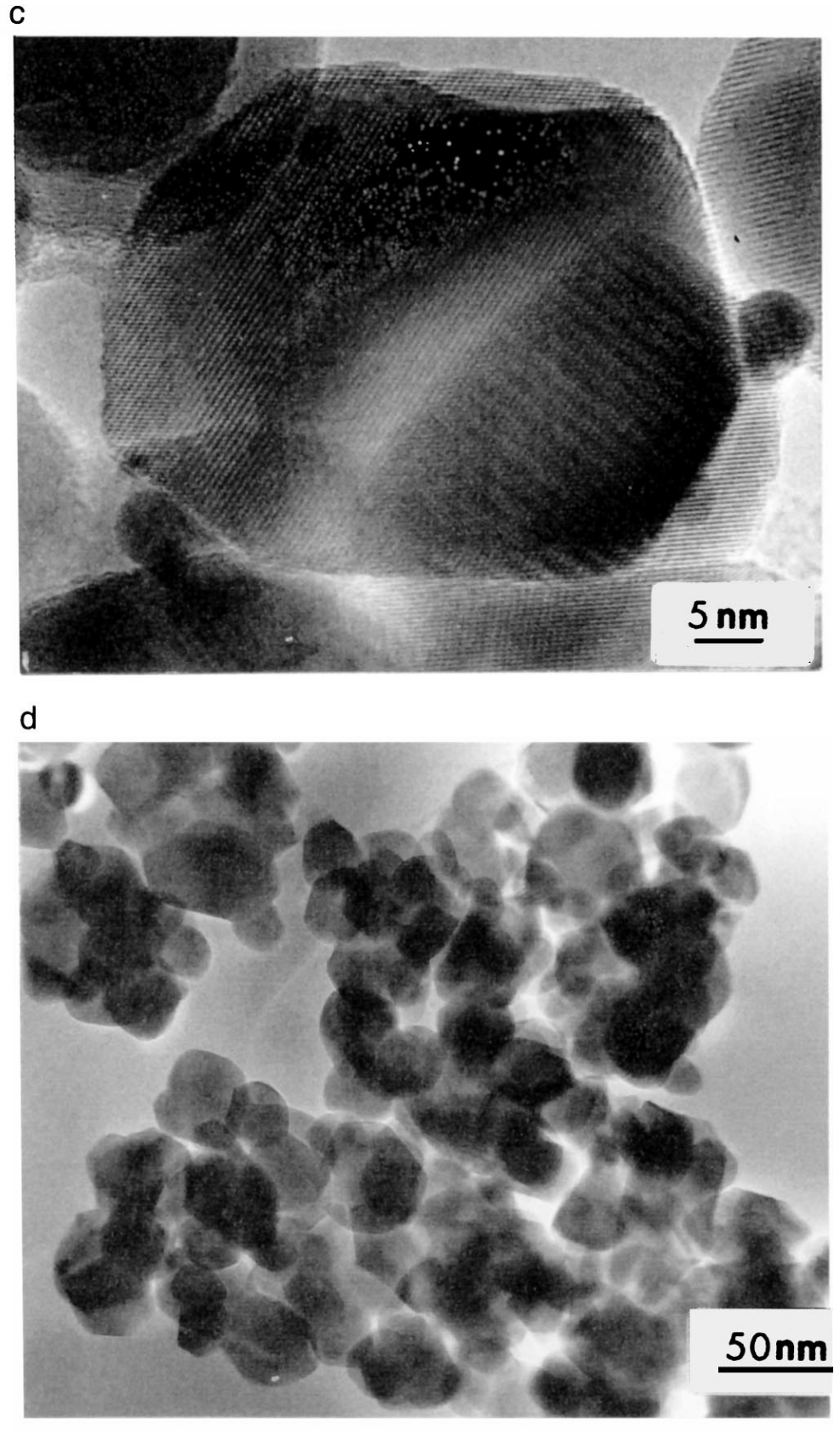

FIG. 2—*Continued*

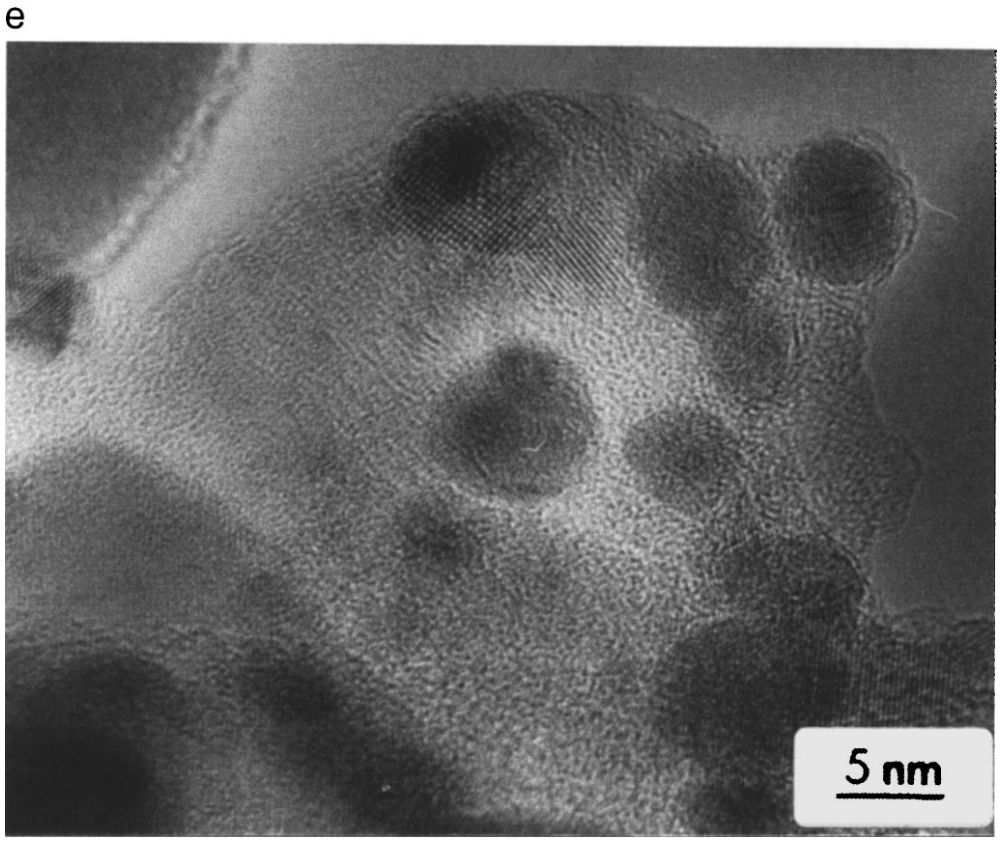

FIG. 2—*Continued*

crystallites required for titration measurements. It appears that such crystallite size effects on methane oxidation rates reflect, instead, an increase in the binding energy of oxygen atoms on PdO_x surfaces as crystallite size decreases.

The proposal that Pd–O bond energy and reactivity decrease as PdO crystallites become smaller is consistent with temperature-programmed reduction of PdO_x/ZrO_2 catalysts with dispersions between 0.107 and 0.381 (Fig. 3). Samples with high dispersion reduce in H_2 at slightly higher temperatures, suggesting that the initial formation of the oxygen vacancies required for H_2 dissociation and for incipient PdO reduction becomes more difficult on small PdO_x crystallites. Temperature-programmed reduction of PdO_x crystallites with methane also shows that reduction occurs at slightly lower temperatures as crystallite size increases. Reduction in methane, however, appears to be controlled by very strong inhibition effects of the water formed during reduction, and provides a less direct correlation with Pd–O bond energies. Briot and Primet (15) have reported that methane oxidation at 873 K on PdO/Al_2O_3 leads to PdO agglomeration; the resulting larger particles give higher methane oxidation rates and reduce (in H_2) at lower temperatures. The higher reactivity of larger PdO particles on Al_2O_3 is consistent with our results on PdO/ZrO_2 and PdO/Al_2O_3 catalysts (Fig. 1). Muller *et al.* (24) also reported an increase in methane oxidation turnover rates as Pd metal crystallites sintered with increasing prereduction temperature of PdO/ZrO_2 prepared from Pd–Zr alloy precursors. Oxygen chemisorbed on smaller Pd crystallites reacted with CH_4 at lower temperatures than on larger crystallites, but

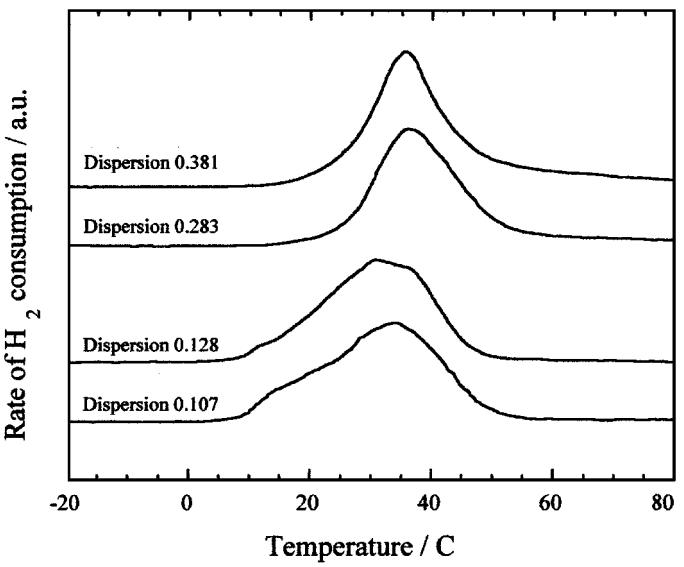

FIG. 3. Temperature-programmed reduction (TPR) of PdO_x/ZrO_2 catalysts using 20% H_2 in Ar (50 cm^3 min^{-1}, 3 K min^{-1}, 0.107–0.381 dispersion range).

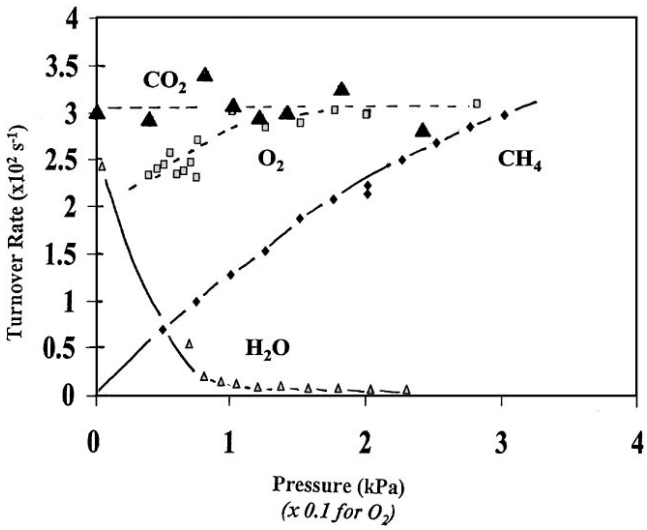

FIG. 4. Effects of CH_4, O_2, H_2O, and CO_2 on methane oxidation rates at low temperatures (553 K, 0.86 wt% Pd/ZrO_2, dispersion 0.381).

the opposite trend was observed when H_2 was used as the reductant. It is possible that the different reduction pretreatments required to vary crystallite size in the study of Mueller *et al.* (24) introduce structural modifications or incomplete reoxidation, which can influence methane oxidation rates.

3.2. Methane Oxidation Kinetic Rate Equations and Reaction Pathways

The effects of CH_4, O_2, CO_2, and H_2O concentrations on methane oxidation rates are shown in Fig. 4. Methane oxidation rates on Pd/ZrO_2 (1.0 wt%) depend weakly on O_2 concentration (0.1 ± 0.1 order), but they are proportional to CH_4 concentration (1.1 ± 0.1 order), in agreement with previous studies (4,5,9). Methane oxidation rates decrease with increasing H_2O concentration, whether water is added to the reactants or formed during reaction (9,25). This suggests that species derived from the readsorption of H_2O are the most abundant surface intermediates during catalysis. Methane oxidation rates are described accurately by a rate expression of the form

$$r = k(CH_4)^{1.0}(O_2)^0(H_2O)^{-1.0}. \quad [1]$$

CO_2 inhibits methane oxidation only when CO_2 concentrations are high (>3–5 mol%) and well above H_2O molar concentrations. Then, reaction rates become proportional to $(CO_2)^{-2}$, as also reported by Ribeiro *et al.* (9).

These kinetic data are consistent with the elementary reaction steps shown in Schemes 1 and 2, where the asterisks stand for oxygen vacancies on PdO surfaces. This elementary step sequence resembles Mars–van Krevelen reduction–oxidation pathways (26) and it includes a rate-determining step involving the dissociative chemisorption of CH_4 on a site pair consisting of adjacent Pd surface vacancies and surface Pd–O species (Scheme 2). This mechanism is consistent with the unusual form of the observed rate expression, which we were unable to predict using other elementary step sequences and rate-determining step assumptions. The sequence of elementary steps in Scheme 1 predicts the observed zero-order oxygen rate dependence and the inhibitory effect of water. This proposed mechanism avoids the need for the coexistence of a separate Pd metal phase in atomic contact with PdO_x during methane oxidation.

The coexistence of PdO_x and Pd crystallites at steady state can be ruled out on thermodynamic grounds. Their coexistence as unstable transient structures during steady-state catalysis is unlikely, because of kinetic barriers and structural rearrangements required for the nucleation of a new phase during each catalytic turnover and because such phase transformations would lead to oscillatory behavior not detected during methane oxidation at low temperatures. Farrauto *et al.* (27) have shown that methane oxidation does not occur under conditions leading to Pd metal and that the slow reoxidation of Pd metal during methane combustion leads to the observed hysteresis in catalytic activity as reactors are cycled between oxidizing and reaction conditions. Their studies show that the Pd metal phase formed under reducing reaction conditions leads to loss of activity. Reoxidation occurs very slowly and with the recovery of activity during the oxidizing part of these cycles. Our proposed mechanism introduces a Pd site into the reaction sequence by postulating the presence of oxygen vacancies on PdO_x surfaces; these vacancies are regenerated at the end of a catalytic cycle by recombination of surface hydroxyl groups formed in C–H bond activation steps (Schemes 1 and 2).

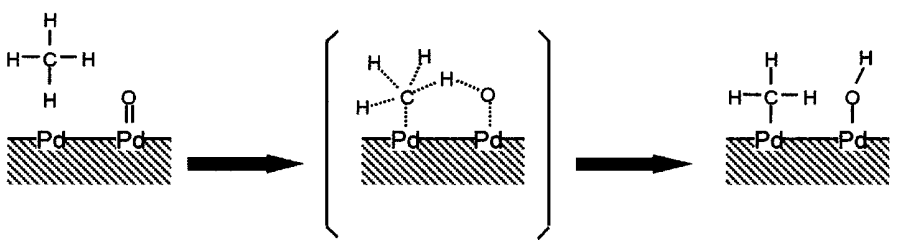

SCHEME 1. Methane dissociation on a surface Pd–PdO site pair.

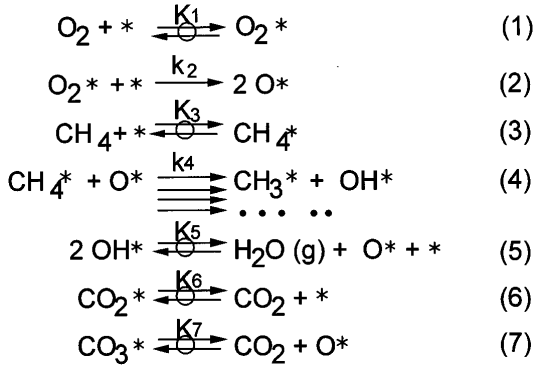

SCHEME 2. Proposed reaction pathways for the oxidation of methane on PdO_x crystallites *Coordinatively unsaturated surface Pd atoms shown schematically in Scheme 1.

In this sequence of elementary steps, carbon atoms in gas phase or physisorbed CH_4 interacts with coordinatively unsaturated Pd sites (∗) on the surface of PdO crystallites (reaction 3, Scheme 2) and H atoms are abstracted sequentially from adsorbed CH_4 by neighboring Pd–O surface species to form surface hydroxyl groups (Pd–OH). The dissociative chemisorption of O_2 (step 2) is assumed to be irreversible based on the absence of O_2 desorption from PdO below 800 K and on the negligible rate of $^{18}O_2$–$^{16}O_2$ equilibration during methane combustion at 553 K (28). The initial H-abstraction step (reaction 4) becomes rate determining when OH∗ species are the most abundant surface intermediates (masi), because it is the only irreversible step involving the masi (17). Subsequent hydrogen-abstraction steps are also irreversible, but kinetically insignificant, because they do not involve masi species. Surface vacancies (∗) are regenerated by quasi-equilibrated condensation of Pd–OH species to form water (reaction 5). Quasi-equilibrated desorption of CO_2 leads to the formation of a vacancy (∗) or a surface oxygen species (O∗), depending on which of these two species provides the binding site for CO_2 (reactions 6 and 7). The observed inhibition by water molecules (or CO_2 at high concentrations) is caused by their tendency to reverse their desorption and titrate both vacancy (∗) and oxygen (O∗) surface sites required for methane activation.

A pseudo-steady-state treatment of the sequence in Scheme 2 confirms that C–H bond activation steps after reaction 4 and oxygen chemisorption steps are not kinetically significant and leads to a complex kinetic rate expression:

$$r = \frac{k_2K_1[O_2]}{3\left[1 + K_3[CH_4] + \frac{k_2K_1[O_2]}{3k_4K_3[CH_4]} + K_1[O_2] + \left(\frac{k_2K_1[O_2][H_2O]}{3k_4K_3K_5[CH_4]}\right)^{0.5} + \left(\frac{1}{K_6} + \frac{k_2K_1[O_2]}{3k_4K_3K_7[CH_4]}\right)[CO_2]\right]^2}. \quad [2]$$

This rate equation simplifies to the observed experimental rate equation (Eq. [1]) when OH* species are the most abundant surface intermediates:

$$r = \frac{k_4K_3K_5[CH_4]^{1.0}[O_2]^0}{[H_2O]^{1.0}}. \quad [3]$$

Equation [2] can also be reduced to Eq. [4],

$$r = \frac{k_2K_1[O_2]^{1.0}}{3\left[\frac{1}{K_6} + \frac{k_2K_1[O_2]}{3k_4K_3K_7[CH_4]}\right]^{2.0}[CO_2]^{2.0}}, \quad [4]$$

when adsorbed CO_2 (CO_2*) or carbonate (CO_3*) becomes the masi species. Rates then become proportional to $[CO_2]^{-2}$, as shown experimentally by Ribeiro *et al.* (9), but only at CO_2 concentrations above which CO_2 inhibition terms become larger than those of H_2O.

Turnover rates are inhibited reversibly by CO_2 and H_2O because these products titrate vacancies on PdO surfaces via the microscopic reverse of their desorption step during methane oxidation (steps 5–7, Scheme 2). The effects of CH_4, O_2, CO_2, and H_2O concentrations on turnover rate are consistent with rate-determining C–H bond activation on site pairs consisting of a Pd–O and an oxygen vacancy (Scheme 1). The density of such site pairs is controlled by quasi-equilibrated desorption of H_2O and CO_2. As a result, the number of available sites decreases as the concentrations of these products increase.

The catalytic sequence in Scheme 2 would suggest that stronger Pd–O bonds in small PdO clusters or incompletely oxidized PdO_x crystallites can lead to a lower surface density of vacancies and to lower methane oxidation turnover rates. In the previous section, such crystallite size effects were attributed to stronger Pd–O bonds in smaller PdO_x crystallites. The next two sections show how accidental or intentional decomposition of PdO to Pd and its incomplete reoxidation also lead to lower methane oxidation rates, because oxygen-deficient PdO_x crystallites also contain stronger Pd–O bonds than stoichiometric PdO.

3.3. Activation Processes during Methane Oxidation

Several authors have reported initial activation periods, during which methane oxidation rates increase after initial contact between Pd-based catalysts and CH_4/O_2 reactants (6–9,15). These activation phenomena were attributed to structural changes of PdO_x crystallites during reaction (6,7,9,15,16) or to an increase in the oxygen content of PdO_x or Pd metal species during initial contact between reduced catalysts and reactants (28). Garbowski *et al.* (16)

detected structural changes in PdO crystallites supported on alumina after initial reduction–oxidation cycles or catalytic tests by transmission electron microscopy and infrared spectroscopy of chemisorbed CO. These changes were associated with the disruption of strongly interacting PdO–Al_2O_3 species during initial catalyst pretreatment or use. This study concluded, however, that activation is not caused by spreading or roughening of PdO crystallites. Ribeiro *et al.* (9) also concluded that activation is not caused by PdO redispersion on the basis of H_2–O_2 titration and X-ray diffraction studies. Recently, Burch *et al.* (29) have shown that prereduced Pd/Al_2O_3 catalysts absorb oxygen to form PdO_x during an initial activation period after contact with CH_4/O_2 reactants. The similar characteristic times required for oxygen uptake and for catalyst activation suggested that bulk oxidation occurs during reaction and that the catalytic activity of PdO_x increases with increasing oxygen content.

In our study, steady-state turnover rates were preceded by initial induction periods only on PdO/ZrO_2 catalysts prepared by rapid heating (10 K min^{-1}) of $Pd(NH_3)_2(NO_2)_2/ZrO_2$ precursors in air to 773 K (catalyst A, Fig. 5, Table 1). These catalysts showed rate increases (by factors of 2–5) over several hours after initial exposure to reactants. H_2–O_2 titration uptakes and CO oxidation rates were similar before and after methane oxidation (Table 1); therefore, the number of exposed Pd atoms remains constant during activation. Both H_2–O_2 titration and CO oxidation reactions probe the number of exposed Pd atoms on Pd metal surfaces formed by reduction or CO oxidation reactions. Changes in PdO_x surface structure or oxygen content during activation cannot be detected by H_2–O_2 titration or CO oxidation (Table 1), either because these reactions are insensitive to structural changes or because such structural changes are erased by the reduction of PdO_x crystallites. In Section 3.1, however, we concluded that the mild

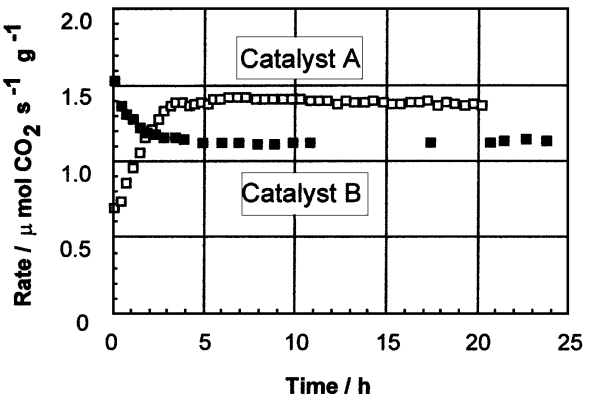

FIG. 5. Methane oxidation rates during initial contact of (1.0 wt%) Pd/ZrO_2 catalysts with CH_4/O_2 (2 kPa/20 kPa) at 553 K. Pd precursor decomposition procedures: catalyst A—10 K min^{-1} to 773 K in air, hold for 24 h; catalyst B—0.5 K min^{-1} to 523 K, 10 K min^{-1} to 773 K in air, hold for 24 h.

TABLE 1

Methane and CO Oxidation Turnover Rates and H_2–O_2 Titration Data on 1% Pd/ZrO_2[a]

Catalyst treatment	H_2–O_2 titration (10^6 surface Pd atoms/g)	Turnover rate ($\times 10^2$ s^{-1})	
		Methane oxidation	CO oxidation
Decomposed in air at 773 K during rapid heating	22.6	1.5	4.0
Steady-state catalyst after 20 h on stream	19.5	6.6	3.5

[a] Methane oxidation: 553 K, 2 kPa CH_4, 20 kPa O_2, 5% conversion; CO oxidation: 393 K, 1 kPa CO, 20 kPa O_2; catalyst A in Fig. 5; pretreatment: 10 K min^{-1} to 773 K in air, hold for 24 h.

reductions used in titration measurements did not modify significantly the dispersion or structure of Pd/PdO species.

Prereduction of fresh catalysts at 773 K led to lower initial methane oxidation rates, which increased during reaction to steady-state values similar to those measured on air-treated samples. These data suggest that initial induction periods are indeed related to oxygen uptake by PdO_x species that intentionally or accidentally become oxygen deficient during the decomposition of impregnated Pd precursor salts.

Transmission electron microscopy of a 4.1 wt% Pd/ZrO_2 sample in the oxidized state did not detect differences in PdO_x structure between fresh and activated catalysts that differed in methane oxidation rates by a factor of 3–4 (cf. Figs. 2a and 2c). The average crystallite diameter of the fresh sample (6 nm) became only slightly larger (6.5 nm) after methane combustion reactions at 553 K for 24 h. Therefore, the increase in turnover rates observed during reaction changes does not appear to reflect structural changes induced by the initial stages of the catalytic reaction.

Controlled decomposition of $Pd(NH_3)_2(NO_2)_2/ZrO_2$ precursors, carried out by increasing the temperature very slowly during oxidation (0.5 K/min vs 10 K/min), eliminates induction periods during methane oxidation (Catalyst B, Fig. 5). Prereduction of these samples in H_2 at 773 K, however, led to very low initial methane oxidation rates and to subsequent activation during methane oxidation. Transmission electron microscopy of samples with higher Pd concentration (4.1 wt%) prepared via slow and fast decomposition failed to detect structural differences between the two samples.

The decomposition of $Pd(NH_3)_2(NO_2)_2$ precursors to PdO occurs as a rapid exothermic process detected as a sharp peak at about 473 K by differential scanning calorimetry. Local high temperatures during decomposition lead to the unintended decomposition of PdO to Pd metal, which occurs even in air at about 1073 K and cannot be reversed completely by reoxidation in air at 773 K (30).

Decomposition of PdO to Pd metal at high temperatures appears to lead to dense Pd metal crystallites, which cannot be oxidized completely even at 773 K in air. Slow heating of precursors during decomposition minimizes temperature excursions and avoids the temporary formation of Pd metal. Oxidation of rapidly decomposed samples (catalyst A, Fig. 5) at 973 K eliminates initial activation periods, confirming that activation is caused by incomplete oxidation after unintended reduction during precursor decomposition. Oxidation at higher temperatures (973 K) in air, or at lower temperatures during reaction, restores oxygen-deficient PdO_x to their active steady state. Similar phenomena are observed when PdO is intentionally decomposed to Pd metal (Section 3.4).

The low methane oxidation turnover rates on oxygen-deficient PdO_x may reflect the presence of stronger Pd–O bonds than on stoichiometric PdO. On supported Pd clusters (31) and Pd single crystals (32), the enthalpy of oxygen chemisorption decreases with increasing oxygen coverage. Also, Pd–O bond energies in stoichiometric PdO are much lower than in oxygen chemisorbed on Pd metal surfaces (33). These data suggest that Pd–O bond energies increase with increasing metallic character of the underlying substrate; similar effects should be observed as PdO_x crystallites become oxygen deficient and this would lead to lower densities of vacancy sites required for rate-determining C–H bond activation steps in methane oxidation. During methane oxidation, oxygen-deficient PdO_x reaches a steady-state extent of oxidation, which becomes, after some time, independent of the initial oxygen content in fresh catalysts.

3.4. Effects of Temperature and Gas Composition Cycles on Methane Oxidation Rates

Several studies have shown that the activity of Pd catalysts in methane oxidation depends on their thermal history (9,10,25,30). In particular, treatments in air at temperatures leading to PdO decomposition to Pd Metal (>1100 K) lead to very low methane oxidation rates (9,25,27,30). Cycling of temperature or gas-phase concentration can also lead to slow transients and irreversible changes in methane oxidation turnover rates on our catalyst samples. For example, PdO decomposition to Pd metal above 1100 K (in air, catalyst B in Table 2), followed by rapid cooling in He to room temperature to prevent reoxidation, leads to very low methane oxidation rates and H_2–O_2 titration uptakes (Table 2).

Diffraction line breadth analysis and transmission electron microscopy studies of samples with higher Pd loading (4.1 wt%), but similar methane oxidation and H_2–O_2 trends after air treatment, detected crystallite growth after PdO-to-Pd decomposition at 1123 K. Pd metal X-ray diffraction lines were not detected on fresh 4.1 wt% Pd/ZrO_2 after reduction in H_2 at 373 K for 1 h. After air treatment at 1123 K and a rapid He quench, sharp Pd metal lines were detected before and after reduction in H_2 at 373 K. The breadth of these lines corresponds to Pd metal crystallite diameters of 47, 36, and 36 nm for the [111], [200], and [220] reflections, respectively. These values are in qualitative agreement with values obtained from titration uptakes (about 100 nm). Electron micrographs also detect large Pd metal crystallites after PdO decomposition to Pd (Fig. 2d); their size becomes similar to those of the ZrO_2 support and the Pd metal particles become detached from the support particles.

TABLE 2

Effect of Pretreatment Temperature and Reduction–Oxidation Environment on Methane Oxidation and H_2–O_2 Titration Dispersion Values (1.0% Pd/ZrO_2)

Catalyst/pretreatment	Pd dispersion (%) from H_2–O_2 titration	Methane oxidation[a] turnover rate (10^2 s^{-1})
A. Fresh catalyst; air/773 K	20.7	6.6
B. Catalyst A; then air, 1123 K	2.5	1.2
C. Catalyst B; then air, 973 K	21.8	0.3
D. Catalyst C, then H_2, 773 K and activation in CH_4/O_2 reactant stream	18.4	5.6

[a] 2 kPa CH_4, 20 kPa O_2, 553 K, 5% methane conversion.

Oxidation of these inactive catalysts in air at 973 K restores Pd dispersions to the values measured on fresh catalysts, but methane turnover rates remain low (catalyst C, Table 2). X-ray line breadth measurements and TEM analyses of 4.1% Pd/ZrO_2 samples pretreated by the same procedures as catalysts B and C detect the redispersion of Pd particles to smaller PdO crystallites during oxidation at 973 K. The TEM and diffraction data discussed below refer to samples prepared by the protocols of Table 2, but containing 4.1 wt% Pd; these samples show catalytic trends similar to those reported for 1.0% Pd/ZrO_2 samples in Table 2. Pd metal X-ray diffraction lines for catalysts C after mild reduction are significantly broader than before oxidation treatment at 973 K (catalyst B). Electron microscopy confirms this redispersion (Fig. 2d vs Fig. 2e) and shows that the average PdO crystallite diameter in catalyst C is 5.7 nm, a value almost identical to that measured for fresh samples (6.0 nm, Fig. 2a). Redispersed PdO crystallites appear to be segregated to certain regions within the support pellets, as if they had formed by shattering of large Pd metal crystallites during oxidation at 973 K. Reduction of catalyst C in H_2 at 773 K before methane oxidation at 553 K (catalyst D, Table 2) restores, after an initial activation period, steady-state methane oxidation turnover rates to values similar

to those measured on fresh catalysts (catalyst A, Table 2). We find remarkable that the PdO crystallite size and methane combustion reaction rates return to their values in fresh catalysts, even after significant growth and redispersion of Pd and PdO crystallites during high-temperature treatments in air.

These structural changes are consistent with slow "redispersion" of PdO particles during oxidation treatments and with crystallite agglomeration during PdO decomposition to Pd metal at high temperatures. A recent study (30) has shown that abrupt changes in catalytic behavior occur as PdO decomposes to Pd during methane oxidation above 1100 K. Methane oxidation rates on supported PdO catalysts show reproducible hysteresis as they cross the PdO–Pd thermodynamic decomposition temperature at each O_2 partial pressure, as also reported by others (24). This hysteresis is caused by the slow reoxidation of Pd metal to stoichiometric oxides, even at high temperatures (723–823 K). On Pd metal, high oxygen binding energies lead to low densities of site pairs required for C–H bond activation and to low methane oxidation turnover rates (Schemes 1 and 2).

The oxidative redispersion of Pd crystallites formed by PdO decomposition leads to strong interactions between PdO_x and ZrO_2, as also found in Pd/Al_2O_3 (16). These PdO_x–ZrO_2 mixed oxides cannot undergo reduction–oxidation cycles required for methane oxidation turnovers and they reduce in H_2 only above 573 K. Hydrogen treatment at 773 K reduces these stable PdO_x–ZrO_2 crystallites, which then reoxidize during methane oxidation at 573 K slowly and without additional redispersion.

The low specific activity of catalysts that have undergone PdO-to-Pd decomposition arise in part from their low dispersion (Table 2), but their turnover rates are also lower than on fresh catalysts. The incomplete reoxidation of large Pd crystallites during methane oxidation leads to oxygen-deficient PdO_x species, which are less active than PdO_x formed by controlled oxidation of fresh catalysts. This is consistent with the low activity of Pd metal (27,29) and with the low initial reaction rates on PdO_x/ZrO_2 catalysts prereduced to Pd before reaction. The complete reoxidation of such particles to the PdO_x stoichiometry present during steady-state methane oxidation requires significant disruption of the dense Pd particles and the interacting oxides formed during extended high-temperature treatments.

5. CONCLUSIONS

The observed effects of crystallite size, of temperature and gas-phase cycling, and of unintended or intentional decomposition of PdO to Pd metal on methane oxidation turnover rates appear to be related to changes in the density and stability of oxygen vacancies on the surface of PdO_x crystallites. The steady-state density of such vacancies depends on the strength of Pd–O bonds, which appears to increase with decreasing PdO_x crystallite size or as crystallites become oxygen deficient. The kinetics of methane oxidation are consistent with a rate-determining step requiring C–H bond activation on a site pair consisting of an oxygen atom and a vacancy site on the surface of PdO crystallites. The density of such vacancies decreases as the crystallite size and the oxygen content of PdO_x decrease. This accounts for the low methane oxidation turnover rates on small PdO_x crystallites and on PdO_x samples that have undergone unintended or intentional decomposition to Pd metal or to oxygen-deficient Pd oxides.

ACKNOWLEDGMENTS

This research has been supported by the Nippon Steel Corporation, the Exxon Education Foundation, and the University of California Energy Institute. One of the authors (K.F.) acknowledges the generous support of the Nippon Steel Corporation for a 2-year sabbatical stay at the University of California at Berkeley. The authors thank Mr. Keif Low for technical assistance in the measurement of methane combustion kinetic orders and Professors Michel Boudart (Stanford University) and Alexis T. Bell (University of California at Berkeley) for helpful discussions and suggestions.

REFERENCES

1. Dalla Betta, R. A., *Catal. Today* **35**, 129 (1997).
2. Lampert, J. K., Kazi, M. S., and Farrauto, R. J., *Appl. Catal.* **14**, 211 (1997).
3. Anderson, R. B., Stein, K. C., Feenan, J. J., and Hofer, L. J. E., *Ind. Eng. Chem*. **53**, 809 (1961).
4. Cullis, C. F., and Willatt, B. M., *J. Catal.* **83**, 267 (1983).
5. Yao, Y. Y., *Ind. Eng. Chem. Prod. Res. Dev.* **19**, 293 (1980).
6. Baldwin, T. R., and Burch, R., *Appl. Catal.* **66**, 337 (1990).
7. Hicks, R. F., Qi, H., Young, M. L., and Lee, R. G., *J. Catal.* **122**, 280 (1990).
8. Hicks, R. F., Qi, H., Young, M. L., and Lee, R. G., *J. Catal.* **122**, 295 (1990).
9. Ribeiro, F. H., Chow, M., and Dalla Betta, R. A., *J. Catal.* **146**, 537 (1994).
10. Burch, R., and Urbano, F. J., *Appl. Catal. A* **124**, 121 (1995); Burch, R., Urbano, F. J., and Loader, P. K., *Appl. Catal. A* **123**, 173 (1995).
11. Cullis, C. F., Nevell, T. G., and Trimm, D. L., *J. Chem. Soc. Faraday Trans.* **68**, 1406 (1972).
12. Benson, J. E., Hwang, H. S., and Boudart, M., *J. Catal.* **30**, 146 (1973).
13. Boudart, M., and Hwang, H. S., *J. Catal.* **39**, 44 (1975).
14. Anderson, J. R., *in* "Structure of Metallic Catalysts," p. 296. Academic Press, New York, 1975.
15. Briot, P., and Primet, M., *Appl. Catal.* **68**, 301 (1991).
16. Garbowski, E., Feumi-Janteau, C., Mouaddib, N., and Primet, M., *Appl. Catal. A* **109**, 277 (1994).
17. Boudart, M., and Djéga-Mariadassou, G., *in* "Kinetics of Heterogeneous Catalytic Reactions." Princeton Univ. Press, Princeton, NJ, 1984; Boudart, M., *AIChE J.* **18**, 465 (1972).
18. Iglesia, E., Barton, D. G., Soled, S. L., Miseo, S., Baumgartner, J. E., Gates, W. E., Fuentes, G. A., and Meitzner, G. D., *Stud. Surf. Sci. Catal.* **101**, 533 (1996).
19. Brus, L., *J. Phys. Chem*. **90**, 2555 (1986).

20. Weber, R. S., *J. Catal.* **151**, 470 (1995).
21. Chou, P., and Vannice, M. A., *J. Catal.* **105**, 342 (1987).
22. Chen, J. J., and Ruckenstein, E., *J. Phys. Chem.* **85**, 1606 (1981).
23. Konig, D., Weber, W. H., Poindexter, B. D., McBride, J. R., Graham, G. W., and Otto, K., *Catal. Lett.* **29**, 329 (1994).
24. Muller, C. A., Maciejewski, M., Koeppel, R. A., and Baiker, A., *J. Catal.* **166**, 36 (1997).
25. Fujimoto, K., Ribeiro, F. H., Bell, A. T., and Iglesia, E., *ACS Div. Petr. Chem. Prepr.* **41**, 110 (1996).
26. Mars, P., and van Krevelen, D. W., *Chem. Eng. Sci.* **3**, 41 (1954).
27. Farrauto, R. J., Hobson, M. C., Kennelly, T., and Waterman, E. M., *Appl. Catal. A* **81**, 227 (1992).
28. Au-Yeung, J., Bell, A. T., and Iglesia, E., unpublished results.
29. Burch, R., Urbano, F. J., and Loader, P. K., *Catal. Today* **27**, 243 (1996).
30. McCarty, J. G., *Catal. Today* **26**, 283 (1995).
31. Zakumbaeva, G. D., and Artamonov, S. V., *React. Kinet. Catal. Lett.* **10**, 183 (1979).
32. Ertl, G., and Rau, P., *Surf. Sci.* **15**, 443 (1969).
33. Kleykamp, H., *Z. Phys. Chem. N.F.* **71**, 142 (1970).